Annals of Nuclear Energy 165 (2022) 108647

Contents lists available at ScienceDirect

Annals of Nuclear Energy

journal homepage: www.elsevier.com/locate/anucene

Quasi-differential neutron induced neutron emissions from ^{235}U, and ^{239}Pu

Kumar S. Mohindroo [a,*], Yaron Danon [a], Ezekiel Blain [a], Matthew Devlin [b], Keegan J. Kelly [b]

[a] Rensselaer Polytechnic Institute, 110 8th St, Troy, NY 12180 USA
[b] Los Alamos National Laboratory, Los Alamos, NM 87545, USA

ARTICLE INFO

Article history:
Received 24 December 2020
Received in revised form 5 August 2021
Accepted 15 August 2021
Available online xxxx

Keywords:
^{235}U
^{239}Pu
Benchmark
Neutron
Emission
Nuclear data
Experiment
Experimental
Simulation
Quasi-differential

ABSTRACT

Uncertainty in nuclear reaction cross sections, angular distributions, and other nuclear data directly impact how well simulations of nuclear systems represent physical observations. To determine how well the nuclear data in ENDF/B-VIII.0, JEFF-3.3, and JENDL-4.0 evaluations describe the physical behaviour of ^{235}U, and ^{239}Pu when subjected to a neutron flux, the neutron emission spectrum was measured for carbon, 93.0% ^{235}U, and 93.9% ^{239}Pu samples, and compared against detailed MCNP6 simulations. The measurements were performed at the Los Alamos Neutron Science Center using a quasi-differential method previously developed at Rensselaer Polytechnic Institute. The measurement spanned 0.82–20 MeV and 30–150 degrees. The measurements show there are a significant number of discrepancies between library predictions of the neutron yield and physical observation. A few of the main discrepancies found are described in this paper. Based on these results a new evaluation utilizing these results for carbon, ^{235}U, and ^{239}Pu is recommended.

1. Introduction

Nuclear data is a crucial input which drives the accuracy of simulation tools used in nuclear reactor design, operation, criticality safety, and nonproliferation efforts. The term nuclear data refers to the collection of cross sections, angular distribution functions, prompt fission neutron spectrum, and other data which describe the interaction of neutrons with particular isotopes. Because nuclear data still holds many uncertain variables, its evaluation is partially dependant on the evaluator, allowing for different evaluators of nuclear data to draw different conclusions. Some nuclear data evaluation projects are, the Evaluated Nuclear Data File (ENDF) (Dunford et al., 2001), the Joint European Fusion Fission library (JEFF) (Koning et al., 2008), and the Japanese Evaluated Nuclear Data Library (JENDL). The latest releases of these evaluation projects are ENDF/B-VIII.0 (Brown et al., 2018), JEFF-3.3 (Plompen et al., 2020), and JENDL-4.0 (Shibata et al., 2011). In 2014, The Collaborative International Evaluated Library Organisation (CIELO) called for an investigation of the nuclear data of several high priority isotopes including ^{235}U and ^{239}Pu (Chadwick et al., 2014). The summary results of CIELO (Chadwick et al., 2018) explicitly state the usefulness of the work discussed in this publication, particularly for the improvement of uncertainties in ^{235}U scattering. A critical review of the evaluation work performed on ^{235}U (Roberto and Andrej, 2018) suggests that there are significant differences between libraries. This work is an implementation of the Rennselaer Polytechnic Institute (RPI) quasi-differential scattering measurement methodology (Saglime et al., 2010). and was used to support the investigation of ^{235}U and ^{239}Pu in the region 0.82–20 MeV. This method is based on performing an experimental measurement of the neutron emission spectrum and comparing it against detailed simulations of the experiment. The methodology provides information on where the nuclear data evaluations differ from one another and on where they differ from the experimental data. By performing the measurement at multiple angles simultaneously, additional information is gained related to the angular distribution of the emission spectrum. Fig. 1 shows a photograph of the detector array from the perspective of facing the neutron beam.

An example of how this information is used is shown by Figs. 3–5 which are taken from Mohindroo (2020) with permission from the author and modified captions. Note that the term (n,xn) refers to the set of reactions (n,2n), (n,3n), (n,4n), etc. It should also be

* Corresponding author.
E-mail address: mohindrooks@ornl.gov (K.S. Mohindroo).

https://doi.org/10.1016/j.anucene.2021.108647
0306-4549/

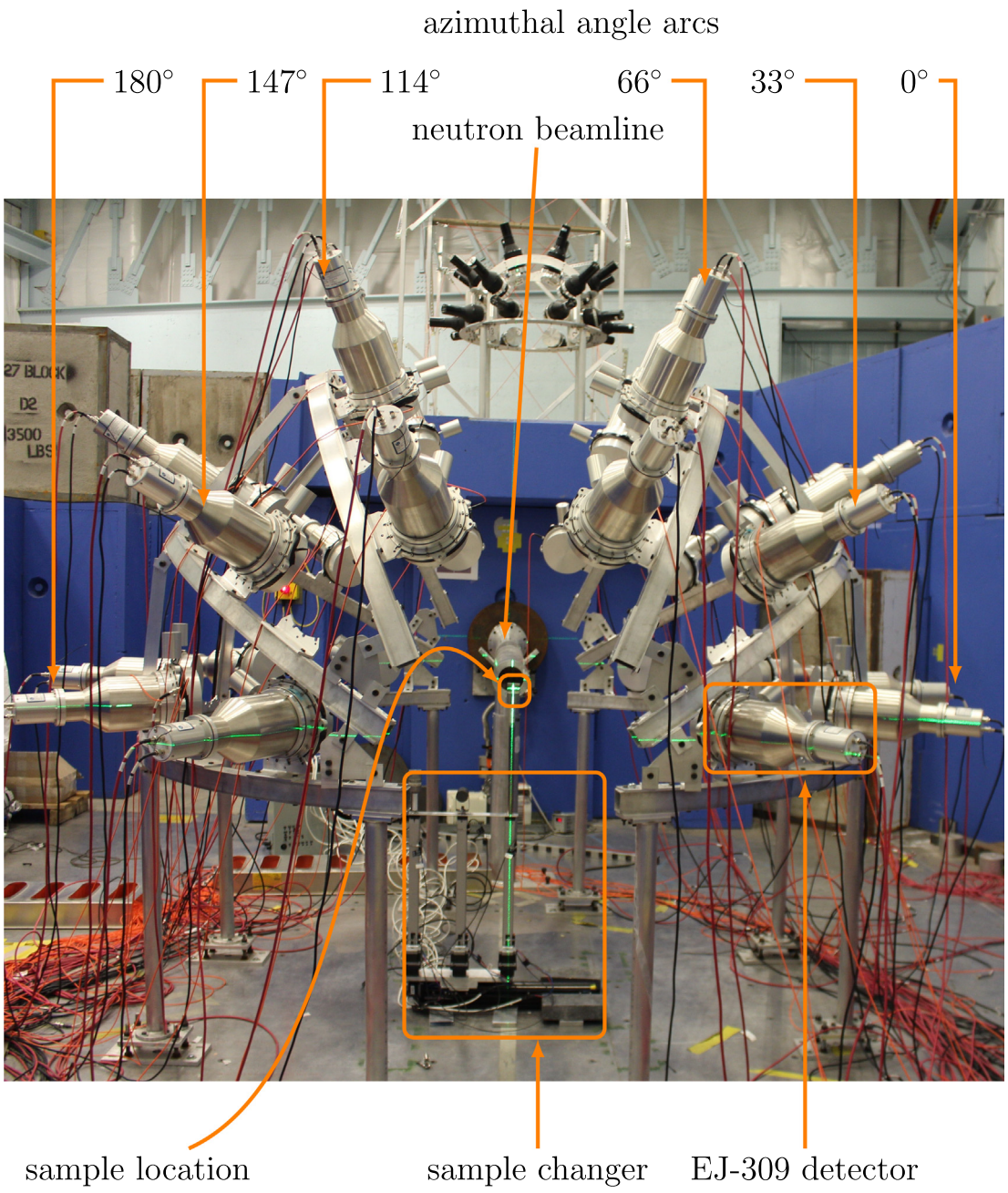

Fig. 1. A photograph of the experimental setup is annotated to mark the sample location, sample changer, an EJ-309 liquid scintillation detector, and the azimuthal angles. The detectors are oriented such that their liquid cell is closest to and perpendicular to the sample. Additional details of the experimental setup are discussed in Mohindroo (2020).

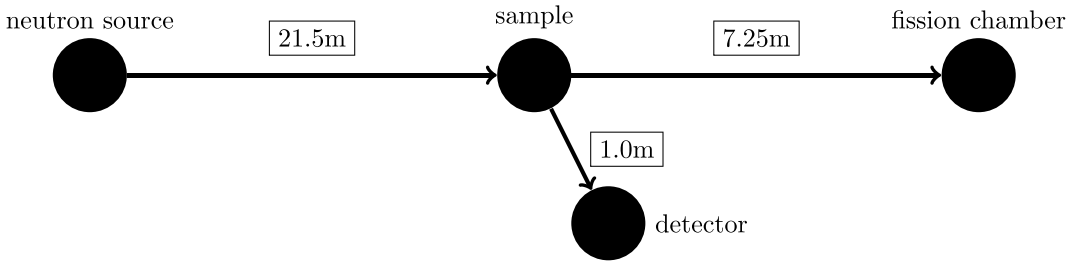

Fig. 2. An illustration showing the relative distance between key locations in the experiment. The sample is 21.5 meters from the neutron source and the detectors are placed along a 1 meter radius surrounding the sample. The fission chamber is placed 28.75 m from the source or 7.25 m from the sample, still in line with the neutron beam.

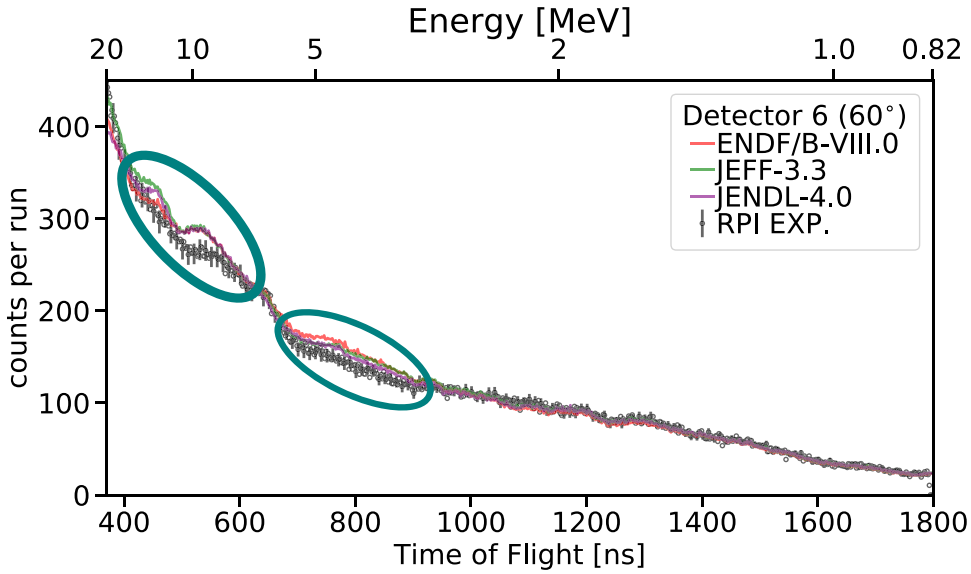

Fig. 3. The ENDF/B-VIII.0, JEFF-3.3, and JENDL-4.0 results in simulation of ^{235}U in detector 6 at 60 degrees are shown. There is an over-estimation between 3.3–6.3 MeV, an over-estimation and shape discrepancy at 10 MeV and a small shape discrepancy at 12 MeV for all evaluations. In addition to the discrepancy between library and simulation, we also see that there are differences between libraries. In this case, JENDL-4.0 performs best in the region of 3.3–6 MeV and ENDF/B-VIII.0 performs best in the region above 10 MeV (Mohindroo, 2020).

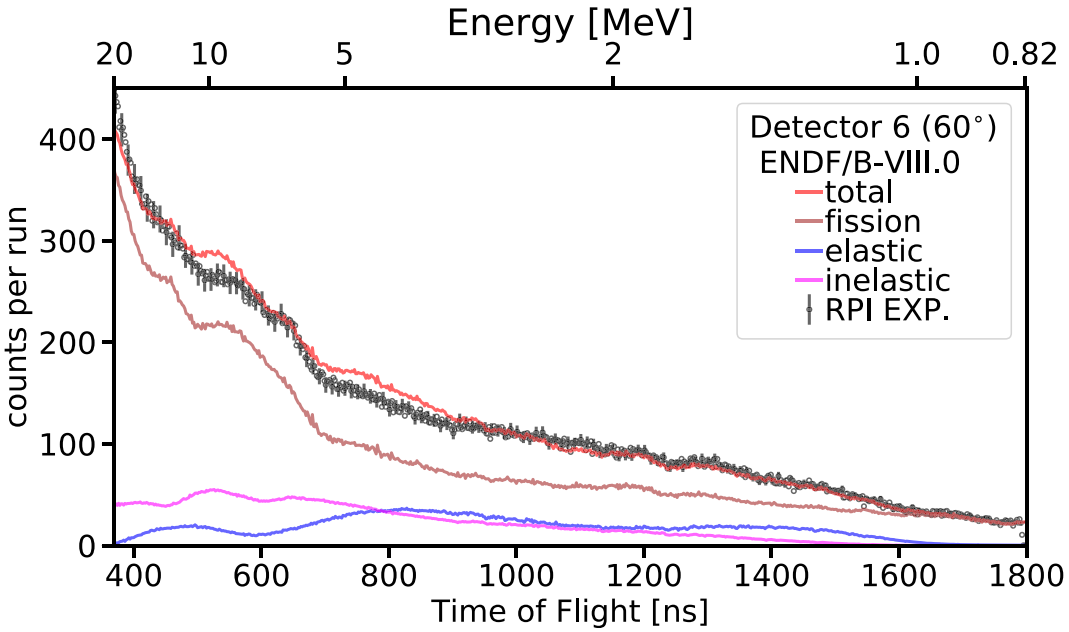

Fig. 4. The simulation contributions for the ENDF/B-VIII.0 simulation of ^{235}U in detector 6 at 60 degrees are shown. The overestimation between 3.3 and 6.3 MeV appears to be related to the increasing fission and inelastic contributions. Note that the inelastic contribution shown here also includes (n,xn) reactions (Mohindroo, 2020).

mentioned that the simulation results shown in these figures were developed using a validated simulation geometry as described later in this paper, as well as in Mohindroo (2020). Fig. 2 is an illustration showing the overview of the experimental setup, indicating distances between relevant points such as the neutron source, sample, detector, and fission chamber. Fig. 3 shows experimental data collected for a detector at 60 degrees compared against ENDF/B-VIII.0, JEFF-3.3, and JENDL-4.0 simulations of the same experiment. This demonstrates how neutron yield changes as a function of energy and also clearly shows how different evaluations can deviate from one another. Fig. 4 separates the ENDF/B-VIII.0 simulation from Fig. 3 into its individual reaction components which can help diagnose the discrepancies observed in the total neutron yield based on observation of the shape of individual contributions as shown in other examples provided by Mohindroo (2020). Comparing Fig. 4–5, which is the same breakdown of the ENDF/B-VIII.0 simulation for a different angle, shows how contributions from individual reactions also change as a function of angle.

When discrepancies are found between libraries, we can observe the cross-sections and angular distributions used in the

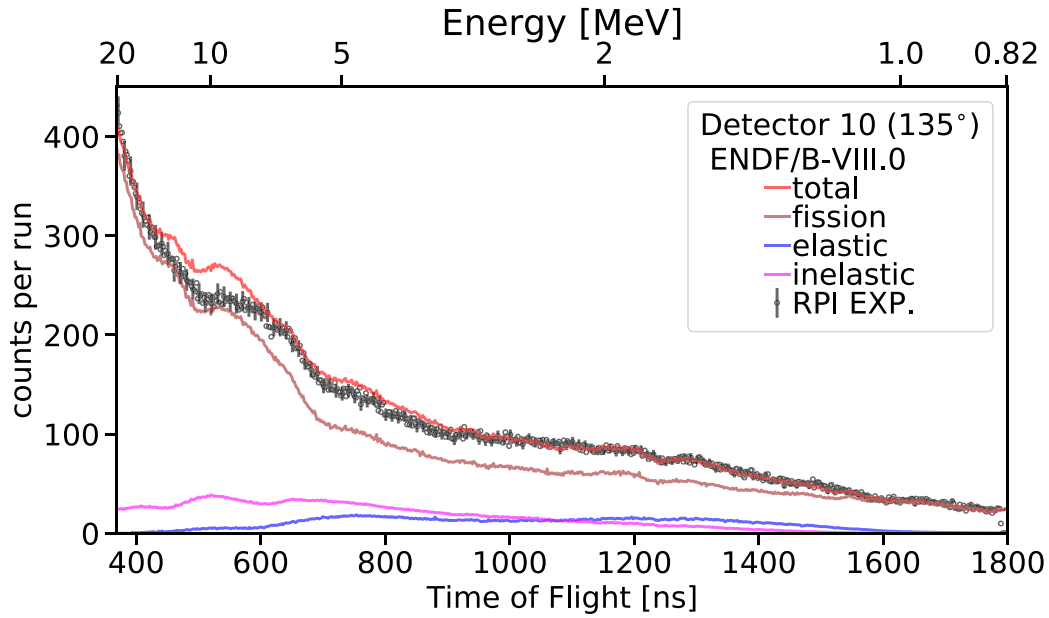

Fig. 5. The simulation contributions for the ENDF/B-VIII.0 simulation of ^{235}U in detector 10 at 135 degrees are shown. The discrepancies in third chance fission near 10 and 12 MeV appear related to contributions from fission and n,2n reactions (Mohindroo, 2020).

best performing library to assist in determining how the evaluations should be updated. The RPI quasi-differential method has been used previously to measure ^{238}U, ^{nat}Fe, Mo, Be, Pb, and Zr (Daskalakis et al., 2017; Daskalakis, 2014; Daskalakis, 2015; Daskalakis et al., 2017; Barry et al., 2013; Youmans et al., 2015). The work on ^{238}U was used by the International Atomic Energy Agency (IAEA) to update their evaluation (Capote et al., 2014). Because the fission contribution in ^{235}U and ^{239}Pu is relatively large, it is more difficult to draw conclusions on neutron scattering as previously done in ^{238}U (Daskalakis, 2014).

An approximation of one collision neutron yield function for this experiment is given in Eq. Equation 1:where E is the energy of the source particle, $\phi(E)$ is the energy dependant neutron flux, Σ_t is the macroscopic total cross section, X is the thickness of the interrogation sample, η is the efficiency of the neutron detector, and E' is the energy of the scattered neutron. The σ_{rx} and f_{rx} are the reaction cross section and reaction angular distribution terms respectively. The generic subscript rx is replaced by s for elastic scattering, inl for inelastic scattering, f for fission, and (n,xn) for (n,xn) reactions. On this fission term, there is an additional $\bar{\nu}$ coefficient which represents the average neutrons generated per fission and on the (n,xn) term there is an x coefficient which represents the order of the (n,xn) reaction. This approximation is suitable for illustrating various aspects which contribute to the angular neutron yield but does not, nor is intended to fully describe the branching behaviour associated with the generation of multiple neutrons at different energies from a single collision, sampling from the prompt fission neutron spectrum, or other complex interactions. The total cross section is considered to be very well known, based on the high accuracy and repeatable nature of transmission measurements. Using this information, coupled with the knowledge of uncertainties for individual reactions, their neutron pro-

$$Y(E,\mu) = \underbrace{\phi(E)}_{\text{neutron flux}} \cdot \underbrace{\left(1-e^{-\Sigma_t(E)X}\right)}_{\text{probability to interact}} \cdot \underbrace{\eta(E')}_{\text{detection efficiency}} \cdot \underbrace{\left(\overbrace{\frac{\overbrace{\sigma_s(E)}^{\text{cross section}}}{\sigma_t(E)} \cdot \frac{\overbrace{f_s(E,\mu)}^{\text{angular distribution}}}{2\pi}}^{\text{elastic scattering}} + \overbrace{\frac{\sigma_{inl}(E)}{\sigma_t(E)} \cdot \frac{f_{inl}(E,\mu)}{2\pi}}^{\text{inelastic scattering}} + \overbrace{\overbrace{\bar{\nu}(E)}^{\substack{\text{average}\\ \text{neutrons}\\ \text{per fission}}} \cdot \frac{\sigma_f(E)}{\sigma_t(E)} \cdot \frac{f_f(E,\mu)}{2\pi}}^{fission} \right)}_{\text{neutron production}} \tag{1}$$

$$\cdot \underbrace{\left(\overbrace{\sum_{x=2}^{N} \overbrace{x}^{\substack{\text{order of}\\ \text{(n,xn)}\\ \text{reaction}}} \cdot \frac{\sigma_{n,xn}(E)}{\sigma_t(E)} \cdot \frac{f_{(n,xn)}(E,\mu)}{2\pi}}^{\text{(n,xn)}} + \ldots \right)}_{\text{neutron production}}$$

duction coefficients and distributions, and their angular distributions, this experiment provides a strong basis by which evaluators can assess how well the balance between individual neutron reactions in each nuclear data evaluation describes physical observation. It should be noted that MCNP6 makes several physics approximations, including in the modeling of fission angular distributions, and neglecting pre-equilibrium fission. These approximations should be acknowledged but the investigation of these effects is beyond the scope of the work described here. Recent experiments also show that there is likely some deficiency associated with the Chi matrix which relates incoming neutron energy to fission neutron output, Nu the neutron multiplicity spectra, and prompt fission neutron spectrum data for ^{239}Pu (Marini et al., 2020). This and other contextual information that describes the state of uncertainty in individual reactions and their angular distributions or neutron production weights should be used when considering the results of this work. Because the data and simulations for this work have been archived, the quasi-benchmark comparison can be updated as our knowledge of related information such as the properties described above improves.

2. Method

The RPI quasi differential method, which was adapted to this work, compares an experimental measurement of the neutron induced neutron emission spectrum to a detailed simulation to assess how well the input nuclear data predicts the observed experimental spectrum. This provides insight on where cross sections or angular distributions may require improvement. A carbon sample is measured in addition to the samples being investigated in order to calculate the normalization between the simulations and experiment and to validate the method. The simulations are performed using nuclear data from different libraries for the samples in order to assess the performance of each library and compare them to one another. Three simulation inputs which must be well characterized to lay the foundation for this methodology are the experimental geometry, neutron flux, and the detector response. The geometry surrounding the sample consists of components such as the aluminum sample changer, aluminum detector array structure, aluminum false floor, vacuum tube, concrete pit, and concrete shielding walls and is very detailed. The neutron flux and detector response inputs will be discussed below.

2.1. Neutron Flux

Creating an accurate simulation is heavily tied to knowing the shape of the neutron flux energy spectrum incident on the sample. The neutron flux was characterized by utilizing a ^{235}U fission chamber (Wender et al., 1993) which was placed 28.75 m from the source. Since the fission cross section of ^{235}U is well known, the response of the fission chamber can be used to determine the shape of the energy spectrum of the neutron flux using Eq. 2.

$$\phi(E_i) = \underbrace{\frac{1}{N \cdot n_t \cdot \zeta}}_{constant} \cdot \frac{C(t_i) - B(t_i)}{\sigma_{U235}(E_i) \cdot \Delta E_i} \tag{2}$$

In this equation $\phi(E_i)$ is the neutron flux in the given energy bin i, N is the number of atoms of the fission chamber material, n_t is the number of triggers from the neutron beam, ζ is the detection efficiency which has been divided by the cross section of the fission chamber target material, $C(t_i)$ is the counts in a given time of flight bin corresponding to the energy bin i, $\sigma_{U235}(E_i)$ is the fission cross-section of ^{235}U which is the fission chamber target material, ΔE_i is the width of the energy bin i, and $B(t_i)$ is the background counts in the time bin i. Since ζ is not dependant on incident neutron energy for a fission chamber and N and n_t are constant, this equation directly provides the shape of the neutron flux energy spectrum. The fission cross section of ^{235}U is considered to be well known. Because the fission chamber is placed at 28.75 m, and the spacing between source pulses is 1.8μs, the low-energy cut point of the flux which we can determine is 1.3 MeV. In order to extend this to lower energies a double exponential was fit to the experimental flux below 15 MeV and used to extend to low energy cut point from 1.3 MeV to 0.25 MeV.

The equation for the fit is shown in Eq. 3:

$$f(E) = A\exp^{-BE}C\exp^{-DE} + F \tag{3}$$

where A, B, C, D, and F are fitting parameters and E is this neutron energy. Light smoothing was applied to the flux and its final form is shown in Fig. 6.

2.2. Detector response

In order to ensure the tally result responds proportionally to the experimental observations, the detector response must be incorporated into the simulation. This is done through a tally multiplier card which multiplies tally contributions from neutrons at a given energy by the probability to detect a neutron at that energy, recreating the detector response. The detector response for each detector as a function of energy was determined by comparing the experimentally observed signal from a 7 cm thick carbon sample to the simulated response. Since the neutron flux was previously determined and the neutron yield is assumed to be well known, dividing the experimental response by the simulated response provides us with the experimental efficiency. The simulated response used in the initial simulation utilized an efficiency generated by a modified version of the SCINFUL code (Dickens, 1988) which was then multiplied by the ratio of experimental/simulated response. This process is represented mathematically in Eq. 4:

$$\begin{aligned} &R_{exp}(E) = \eta(E)\Phi(E)Y(E) \\ &R_{mcnp}(E) = \eta_{scinful}(E)\Phi(E)Y(E) \\ &\rightarrow \eta(E) = \frac{R_{exp}(E)}{R_{mcnp}(E)}\eta_{scinful}(E) \end{aligned} \tag{4}$$

where $R_{exp}(E)$ are the observed experimental counts as a function of energy, $R_{mcnp}(E)$ are the simulated counts as a function of energy, $Y(E)$ is the neutron yield as a function of energy, E is the neutron energy, $\eta(E)_{scinful}$ is the SCINFUL generated efficiency, and $\eta(E)$ is the detector efficiency as a function of energy. The time of flight technique was used to convert the neutron time of flight observed in the experiment and in the simulation into corresponding incident neutron energy. The time of flight equation is given in Eq. 5 and shows the final form of the relationship between kinetic energy and velocity.

$$E(t) = m_0c^2\left(\sqrt{1 - \frac{L^2}{c^2}\frac{1}{t^2}} - 1\right) \tag{5}$$

In this equation $E(t)$ is the kinetic energy of the particle, m_0c^2 is the rest mass of the particle, L is the total length traveled by the particle, c is the speed of light, and t is the time it took for the particle to travel Length L.

The final form of the efficiency used the carbon based efficiency below 8 MeV to incorporate the effects of exact voltage setting, and physical implementation on the low level discriminator. This was then combined with the SCINFUL efficiency from 8 to 30 MeV since the carbon based efficiencies converge and the SCINFUL calculation provides a more accurate description at higher energies. The composite efficiency was then lightly smoothed to remove stitch effects.

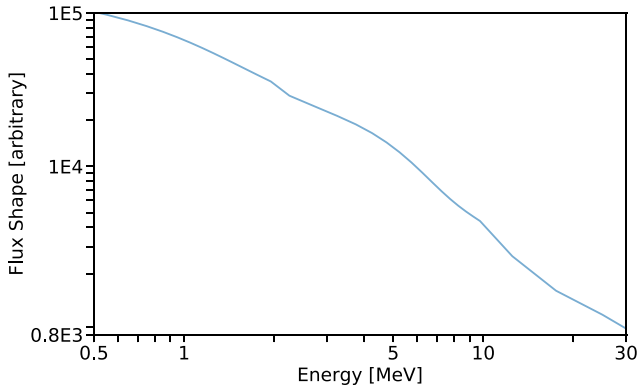

Fig. 6. The final flux used for the MCNP simulations is shown. The flux below 1.3 MeV is generated using a double exponential decay which was fitted to the data below 15 MeV and light smoothing was applied to the total curve.

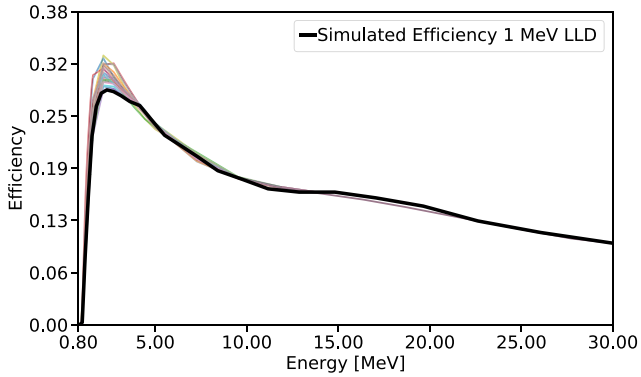

Fig. 7. The 28 individual detector efficiencies are shown and compared against SCINFUL generated efficiency using a 1 MeV low level discriminator.

The individual detector efficiencies for each of the 28 detectors is compared against the SCINFUL efficiencies using a 1 MeV low level discriminator (LLD) in Fig. 7. Each detector has a slightly different response to voltage input and the voltage settings for each detector differ. The deviations in low level discriminator correspond to these deviations in voltage.

3. Experimental details

The neutron induced neutron emission measurements of ^{235}U and ^{239}Pu were performed at the Los Alamos Neutron Science Center (Lisowski and Schoenberg, 2006) (LANSCE) Weapons Neutron Research facility (WNR). The Linear Accelerator (LINAC) is an 800 MeV proton accelerator which generates neutrons by inducing spallation in a tungsten target, Target-4. A white spectrum of neutrons up to 800 MeV are emitted isotropically and collimated into specific beam lines. The beamline used for the experiment is 15 degrees to the left of the incident proton beam known as 15-L and the sample location was 21.5 m from the neutron source. A 0.5″ thick HDPE filter doped to 5 wt% natural boron was placed 11.78 m from the neutron source to remove low energy neutrons which would otherwise arrive at the sample location during a subsequent source pulse. A 1″ thick lead filter was placed 14.53 m from the source in order to reduce the intensity of the gamma flux incident on the sample. The neutron beam was well collimated, and a study was performed which showed that the although the collimation produced a neutron spray, the spray did not effect the net detector response. This allows for the use of a straight beam approximation in the simulations. The diameter of the beam spot at the sample location was 2.73 cm. Since neutron energies of up to 800 MeV are present in the beamline, a time of flight cut was used in post processing to focus on the spectra produced by neutrons 20 MeV and below which arrive after 369 ns. This was done because the primary intent for this work is to serve as a point of comparison for nuclear data evaluations which often only extend to up to 20 MeV. The EJ-309 detectors were held in a hemispherical aluminum structural array (Haight et al., 2012) with each detector face placed 1 m from the sample covering the range 150 to 30 degrees surrounding the sample. The signals from the detectors were digitized using CAEN VX1730B 14 bit digitizers which had a sampling rate of 500 MHz (2 ns/channel). The digitized signal was then sent to the DAQ (data acquisition) computer. The uncertainty in the total flightpath (source to sample + sample to detector) of 22.5 m is assumed to be 0.01 m and the uncertainty in t_0 is determined by the FWHM of the gamma flash to be 4 ns. The dimensions and masses of the samples used are given in Table 1. The 133 g carbon sample was a bare cylinder and the 49.5 g 93% ^{235}U HEU sample was a truncated cone encapsulated in aluminum foil. A duplicate of the aluminum foil was also measured as its blank. The 24.61 g 93.9% ^{239}Pu sample was a Pu-Ga alloy with 3.6at% being Ga (Lynn et al., 1998). The sample was a cylinder double encapsulated in stainless steel. A second sample containing only 0.47 g of ^{239}Pu was used as its blank.

Table 1
Mass and dimensions of samples.

Sample	Mass [g]	Cross-sectional measure	Thickness
carbon	133 ± 0.1	3.81 cm dia. ± 0.01 cm	6.984 cm ± 5 μm
^{235}U	49.5 ± 0.5	d1 2.26 cm ± 0.015 cm d2 1.905 cm ± 0.06 cm	0.889 cm ± 1.27 μm
^{235}U blank	0.7	8.41 cm ± .079 cm x 6.82 cm ± .079 cm	2.286 μm
^{239}Pu	24.61 ± 0.2	2.55 cm dia. ± 0.01	0.307 cm ± 1 μm
^{239}Pu blank	0.47 ± 0.2	2.543 dia. ± 0.01	0.006 cm ± 1 μm

4. Data analysis

The experimental data was recorded using a digital acquisition system and processed into a state which can be compared with the detailed MCNP simulations. The processing steps are given below.

Pulse shape discrimination was performed using the charge integration (Adams and White, 1978) and good separation was observed from 0.82 MeV to 21.31 MeV. The total window of integration is 270 ns long and the tail of the pulse is defined as the last 200 ns of the window. The tail fraction is defined according to Eq. 6.

$$\text{tailfraction} = \frac{\text{tailintegral}}{\text{totalintegral}} \tag{6}$$

The charge integral plot is shown in Fig. 8: which shows the upper and lower integral bounds of the classification region in black, the upper and lower bounds of the clean separation as vertical magenta lines, and the discrimination curve in red. Particles in the upper region are classified as neutrons, and particles in the lower region are classified as gamma rays. After classifying the detection events by particle type the net experimental spectrum was computed. Further details on the pulse shape discrimination method are discussed in Mohindroo (2020).

The net experimental spectrum is determined through Eq. 7:

$$C_{net} = \frac{C_{\text{sample}}}{n_{\text{Sample}}} - \frac{C_{\text{open}}}{n_{\text{open}}} \tag{7}$$

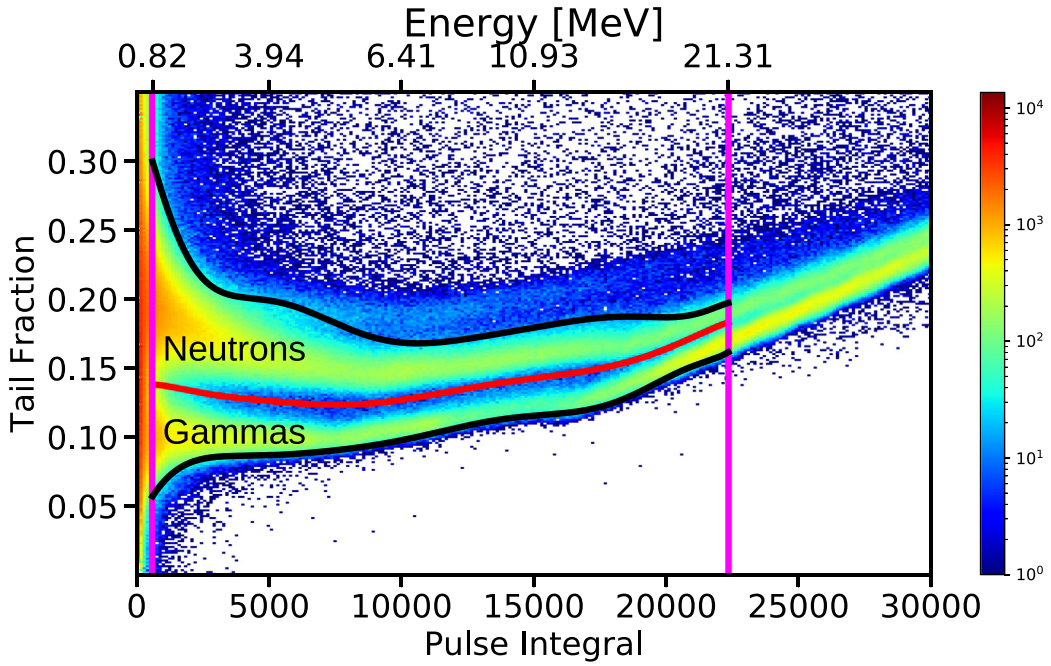

Fig. 8. Charge integral plot for ^{235}U in detector 0 at 150°. The vertical magenta lines encompass the bounds of clean separation. The black curves enclosing the primary data set represent the bounds of classification. The red curve represents the cut line. Particles between the cut line and upper bound are classified as neutrons and particles between the cut line and lower bound are classified as gamma rays.

where C is the counts in a given sample and n are the number of runs available for that sample. The statistical uncertainty of the net spectrum is given by Eq. 8:

$$\frac{\sigma_{net}}{C_{net}} = \sqrt{\frac{C_{\text{sample}}}{(n_{\text{Sample}})^2} + \frac{C_{\text{open}}}{(n_{\text{open}})^2}} \tag{8}$$

where σ is statistical uncertainty of a particular sample.

Finally, the simulation must be normalized to the experiment in order to make an accurate comparison. The normalization factor for a detector is determined by comparing the open subtracted carbon sample to an open subtracted carbon simulation. In the ideal case where the simulation perfectly represents the experimental setting and the nuclear data is exactly known, the normalization value for each detector should be equal. The degree to which these normalization values deviate from one another is a direct measure of the systematic uncertainty associated with the implementation of this methodology. The normalization factor spread for all detectors in the ^{235}U measurement segment is given in Fig. 9, and shows that there are significant differences in the normalization factors at

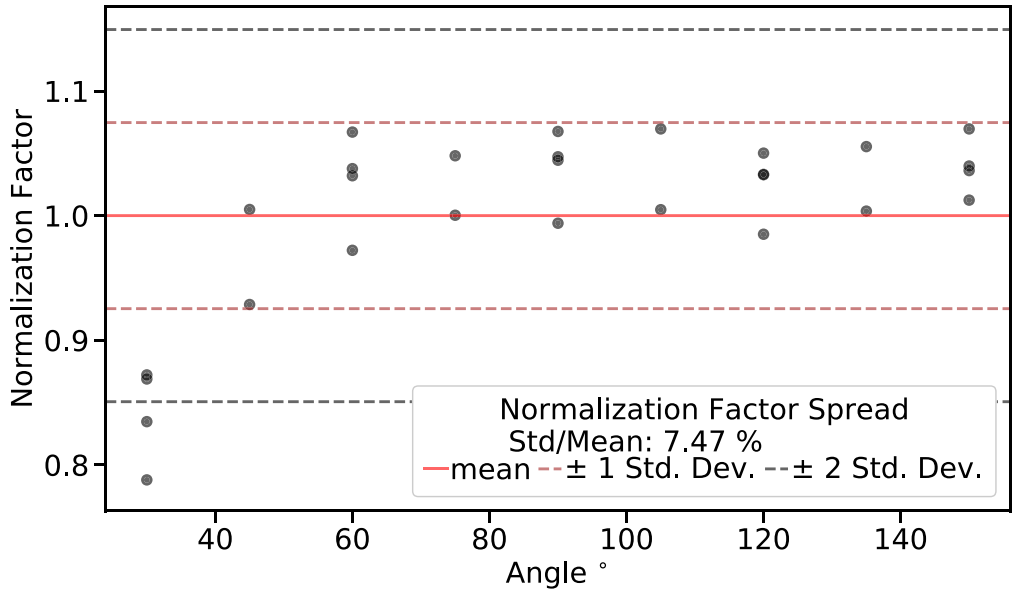

Fig. 9. The normalization factor spread for all detectors shows a 7.47% systematic uncertainty but indicates that there is significant problems with the angular distribution at 30 and 45 degrees.

30 and 45 degrees. Based on the experimental environment this is not believed to be related to geometrical, flux, or efficiency effects, and appears to indicate that there are significant problems in the angular distribution at forward angles. The systematic uncertainty for the forward angle detectors is treated as the 7.47% observed in Fig. 9 and the remaining detectors are observed separately. The normalization factor spread for detectors at angles $\geqslant 60^{\circ}$ is given in Fig. 10 and shows a systematic uncertainty of 2.77%. The corresponding values for the ^{239}Pu systematic uncertainties are 7.55% and 2.85%.

5. Results

After performing the data analysis and developing the simulation inputs, the net experimental spectrum is compared against the net simulated spectrum. The nuclear data characterizing materials which are not the sample are held constant using the ENDF evaluation and the simulation is performed multiple times, using the nuclear data from a different evaluation to characterize the sample in each case. This allows us to observe the agreement or differences between libraries based purely on their characterization of the sample nuclear data. The evaluations used were ENDF/B-VIII.0, JEFF-3.3, and JENDL-4.0. Additionally, the ENDF/B-VIII.0 simulation is broken into its separate reaction contributions. This is done by using the nonu card to remove fission when applicable. The tally tag method can then be used to tag the elastic scattering contribution of the non fission spectrum. The remaining contribution is labeled as inelastic, but it does include contributions from (n,xn) reactions as well. These results were assessed for each of the 28 detectors which were placed at 30, 45, 60, 75, 90, 105, 120, 135, and 150 degrees surrounding the sample. The following discussion of the results is intended to highlight and provide examples of the discrepancies found.

5.1. Carbon

The experimental neutron emission spectrum from Carbon, and the ENDF/B-VIII.0, JEFF-3.3, and JENDL-4.0 simulations for detectors placed at 30, 75, 90, and 150 degrees are given in Fig. 11 to show how the emission spectrum varies across angles.

A thorough review of the carbon results revealed discrepancies in the nuclear data. Most notably, the region between 2–2.65 MeV in detectors $\geqslant 60$ degrees was not predicted well by the simulations and previous work (Daskalakis, 2015) also showed similar findings. This is thought to be a cross section discrepancy based on its presence at most angles. The region between 3.3–4.2 MeV at 90, 105, and 120 degrees was over-predicted by simulations with ENDF/B-VIII.0 performing closest to the experiment, JEFF-3.3 and JENDL-4.0 were discrepant up to 5 MeV. This is thought to be an angular distribution problem due to it being present only at a few central angles.

These discrepancies identified in carbon were compared against trends in the efficiency, neutron flux, and the results for the ^{235}U and ^{239}Pu samples, and showed no correlation between them. This suggests that these discrepancies are derived from the cross sections and angular distributions describing carbon neutron reactions in carbon and should be addressed moving forward.

5.2. ^{235}U

The experimental neutron emission spectrum from ^{235}U, and the ENDF/B-VIII.0, JEFF-3.3, and JENDL-4.0 simulations for detectors placed at 30, 75, 90, and 150 degrees are given in Fig. 12 to show how the emission spectrum varies across angles. At 30 degrees the simulations predict systematically low but remain within experimental uncertainty. The large uncertainty at this angle is reflective of the increased systematic uncertainty for forward angle detectors discussed previously. The detectors at 75, 90, and 150 degrees show examples of the two primary discrepancies identified in the ^{235}U result which are over-predictions between 3.3–5 MeV and between 10–12 MeV. It should be noted that the authors from reference (Daskalakis, 2014) did not find such discrepancies near 10–12 MeV. Fig. 13 shows the effect of room return and indicates that it does not heavily influence the shape of the spectrum in the discrepant regions. Room return is the effect of neutrons scattering from the sample to components in the room and scattering back to be detected.

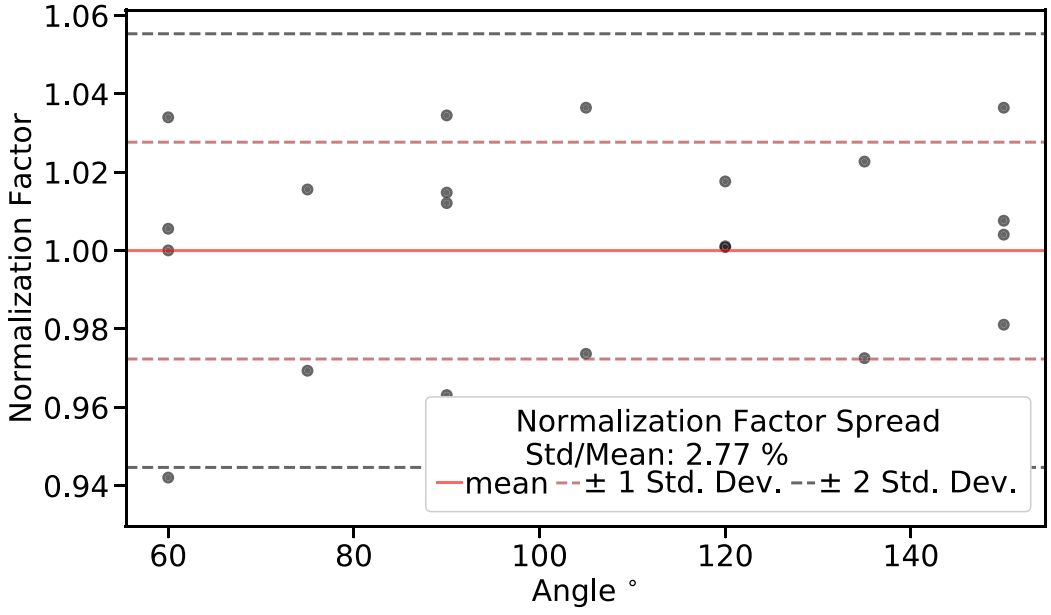

Fig. 10. The normalization factor spread for non forward angle detectors shows a 2.77% systematic uncertainty.

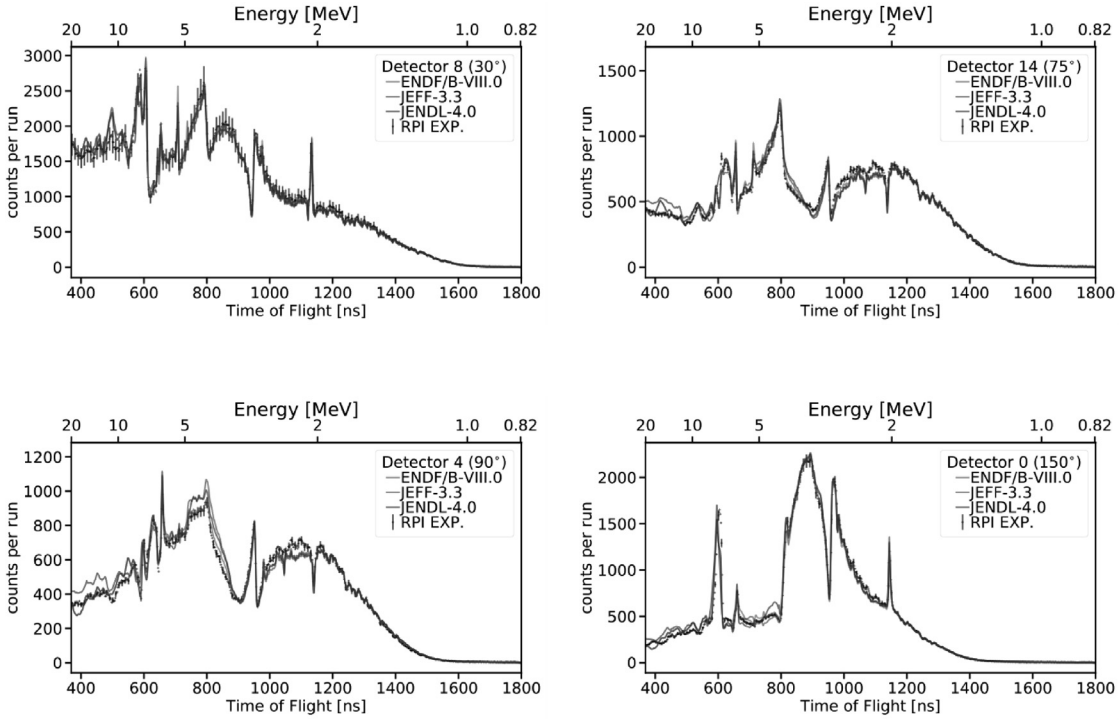

Fig. 11. The Carbon results at 30, 75, 90, and 150 degrees show representative examples of the discrepancies found in carbon. The simulation generally predicts the emission spectrum well but is discrepant in isolated areas for different angles.

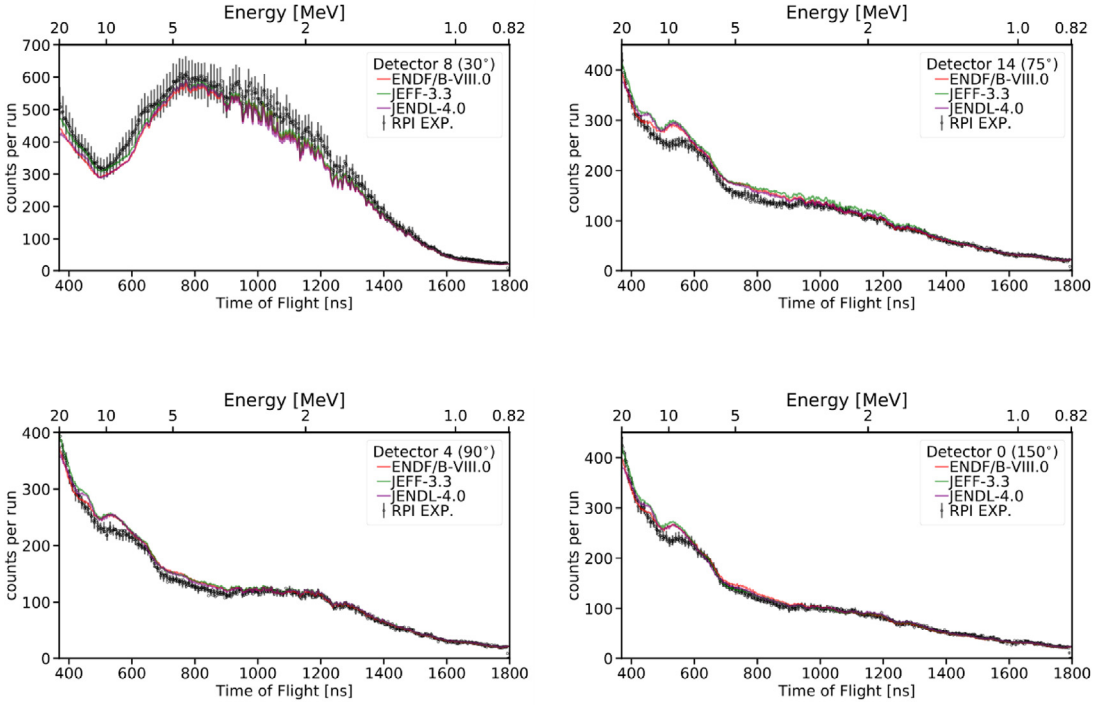

Fig. 12. The ^{235}U results at 30, 75, 90, and 150 degrees show representative examples of the discrepancies found in ^{235}U. The simulations are systematically low at 30 degrees but remain at the edge of uncertainty. Note that the large uncertainty at 30 degrees are reflective of the normalization factor behaviour noted in the discussion of systematic uncertainty for forward angle detectors. At angles $\geqslant$60 degrees the simulations over-predict in the region between 3.3–5 MeV and 10–12 MeV. JEFF-3.3 also shows some over-prediction between 2–3.3 MeV at 75 degrees.

The over-predictions between 3.3–5 MeV and 10–12 MeV occur at all angles $\geqslant$60 degrees. At 75 degrees JEFF-3.3 also over-predicts to as low as 2 MeV. The features at 10 and 12 MeV are believed to be related to the third-chance fission step which occurs near 12 MeV. ENDF/B-VIII.0 tends to predict the 12 MeV feature most accurately. There is a possibility that the discrepancy observed in

third-chance fission is related to the energy distribution of emitted particles during the (n,2n) and fission processes and further steps should be taken to investigate this.

5.3. ^{239}Pu

The experimental neutron emission spectrum from ^{239}Pu, and the ENDF/B-VIII.0, JEFF-3.3, and JENDL-4.0 simulations for detectors placed at 30, 90, 120, and 150 degrees are given in Fig. 14 and indicate several localized discrepancies between the data and simulations. There is an under-prediction between 5–10 MeV at 30 degrees. The high uncertainty at this angle is reflective of the trend identified in normalization factors previously discussed in the systematic uncertainty section. A discrepancy similar to the one identified in ^{235}U between 3.3–5 MeV at angles $\geqslant$60 degrees is present in ^{239}Pu at 75 and 90 degrees only and JENDL-

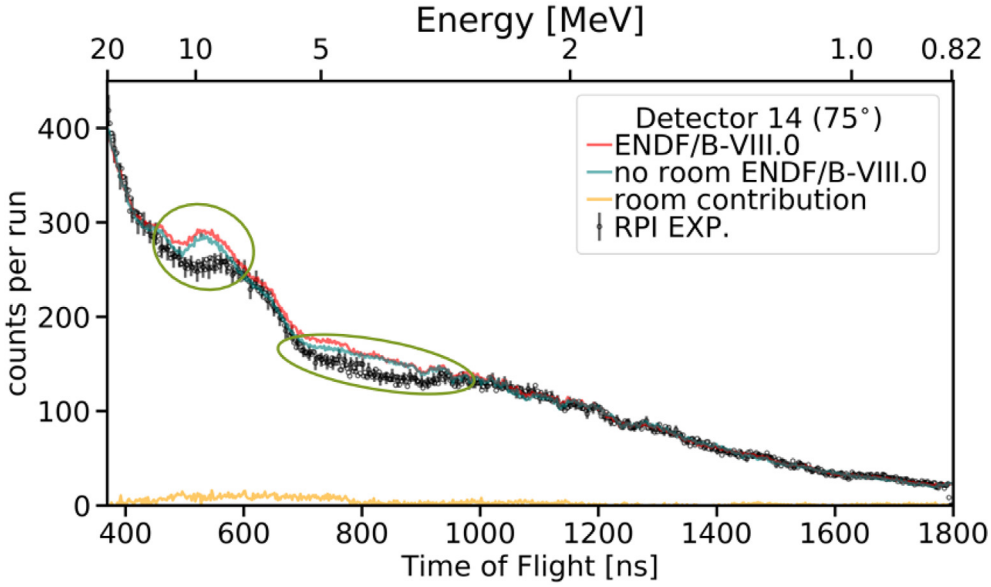

Fig. 13. The ^{235}U room return effect for detector 14 at 75 degrees shows that the two primary discrepancies found in ^{235}U at angles $\geqslant$60 degrees are not heavily influenced by secondary neutron yields. The no room simulation removes all geometrical components modeled within the simulation except for the in-beam filters and the sample.

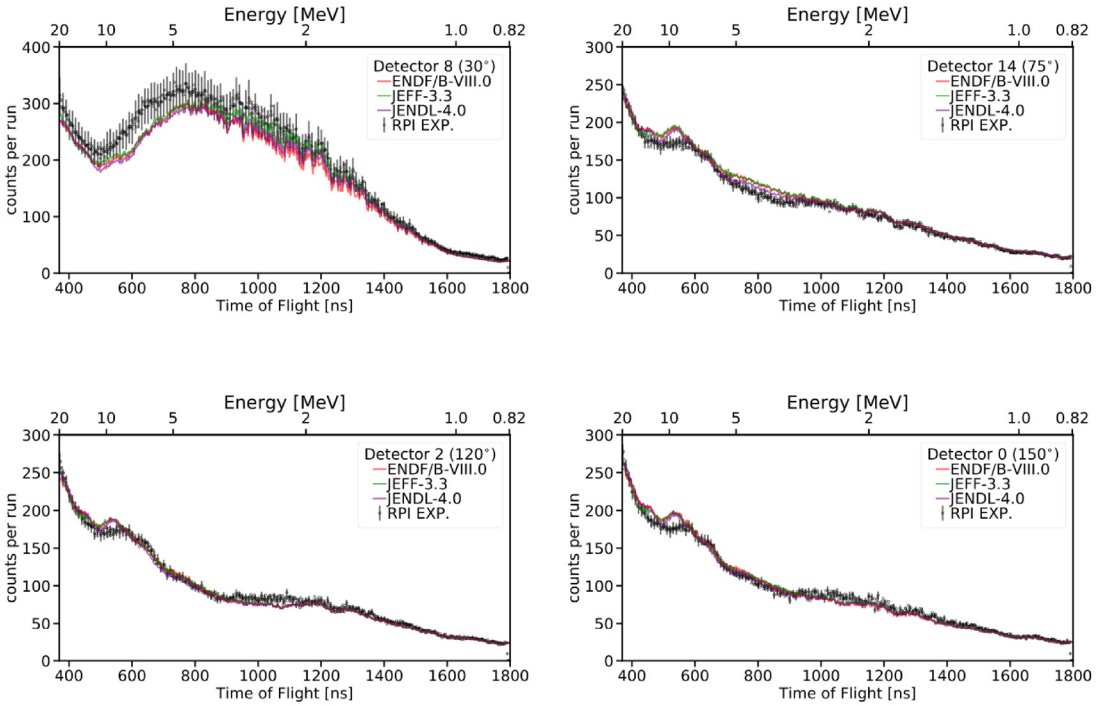

Fig. 14. The ^{239}Pu results at 30, 75, 120, and 150 degrees show representative examples of the discrepancies found in ^{239}Pu. The simulations under-predict between 5–10 MeV at 30 degrees and this discrepancy is only seen at this angle. Note that the large uncertainty at 30 degrees are reflective of the normalization factor behaviour noted in the discussion of systematic uncertainty for forward angle detectors. The results at 75 degrees show that the simulations over-predict in the region between 3.3–5 MeV and 10–12 MeV. The over-prediction between 3.3–5 MeV also occurs at 90 degrees and in each case JENDL-4.0 performs best. The results at 120 degrees show an under-prediction near 2.5 MeV which is also present at 45 degrees. The simulations at 150 degrees appear systematically low below 3.3 MeV but are close to the edge of uncertainty.

4.0 performs significantly better than the other libraries in this region. The 10 and 12 MeV discrepant features are also present in ^{239}Pu at angles $\geqslant$60 degrees but appear less severe than as seen in ^{235}U and all evaluations predict these features roughly the same. The results at 120 degrees show there is an under-prediction between 2–3.3 MeV and this effect is also present at 45 and 150 degrees. The simulations at 150 degrees also show under-prediction below 2 MeV.

6. Conclusion

An experiment was performed to investigate the neutron emissions from ^{235}U and ^{239}Pu samples at LANSCE WNR and a carbon sample was also measured for validation purposes. The quasi differential scattering method developed at RPI was adapted to compare the experimental results to detailed MCNP simulations. Differences were found between the experiment and simulations in the carbon, ^{235}U, and ^{239}Pu samples. The discrepancies identified in each sample are not correlated and manifest at different angles and energies except for the problem related to the third-chance fission step which is present in both ^{235}U and ^{239}Pu at angles $\geqslant$60 degrees.

In carbon, under-prediction occurs in the region between 2–2.65 MeV for all libraries at angles $\geqslant$60 degrees and previous experiments have shown problems predicting this region in the past (Daskalakis, 2015). Over-prediction occurs in the region between 3.3–4.2 MeV at 90, 105, and 120 degrees and libraries are discrepant, with ENDF/B-VIII.0 performing best. There is also over-prediction between 10–13 MeV at all angles except 60 and 75 degrees and the libraries are discrepant, with ENDF/B-VIII.0 performing best. The simulated contributions show in some localized cases that particular portions of the over-prediction are explicitly due to the shape of inelastic or elastic contributions. The differences found between 15–20 MeV were shown to be heavily tied to the elastic scattering contribution and appear to be an angular distribution problem.

In ^{235}U the region between 3.3–5 MeV shows over-prediction by all libraries at angles $\geqslant$60 degrees which appears to be related to the rising fission and inelastic contributions. The differences at 10 and 12 MeV related to third-chance fission also appear to be heavily influenced by the fission and inelastic contributions.

In ^{239}Pu there is an under-prediction at 30 degrees between 5–10 MeV for all libraries, over-prediction at 75 and 90 degrees between 3.3–5 MeV for all libraries, and the over-prediction at angles $\geqslant$60 degrees at 10 and 12 MeV for all libraries. The differences between 3.3–5 MeV at 75 and 90 degrees appear to be related to the rising fission and inelastic contributions as seen in ^{235}U and JENDL-4.0 performs better than the other libraries. The third-chance fission features at 10 and 12 MeV are heavily dominated by the fission contribution and show that holding this constant means that nearly any contribution from elastic or inelastic components at 10 MeV would result in over-prediction of the experimental data. It is recommended that re-evaluation for carbon, ^{235}U, and ^{239}Pu be performed utilizing this data.

CRediT authorship contribution statement

Kumar S. Mohindroo: Conceptualization, Methodology, Software, Validation, Formal analysis, Investigation, Data curation, Writing - original draft, Visualization. **Yaron Danon:** Conceptualization, Methodology, Resources, Writing - review & editing, Funding acquisition, Supervision, Project administration. **Ezekiel Blain:** Conceptualization, Methodology, Resources, Writing - review & editing, Funding acquisition, Supervision. **Matthew Devlin:** Resources, Funding acquisition, Supervision, Project administration. **Keegan J. Kelly:** Resources.

Declaration of Competing Interest

The authors declare that they have no known competing financial interests or personal relationships that could have appeared to influence the work reported in this paper.

Acknowledgements

The work at Los Alamos National Laboratory was performed under the auspices of the US Department of Energy under Contract No. 89233218CNA000001.

The first author was supported by the Nuclear Regulatory Commission Fellowship Program under the grant NRC–HQ-84–15-G-0018 Program B.

References

Adams, J., White, G., 1978. A versatile pulse shape discriminator for charged particle separation and its application to fast neutron time-of-flight spectroscopy. Nuclear Instruments and Methods 156, 3, 459. https://doi.org/10.1016/0029-554X(78)90746-2. url:http://www.sciencedirect.com/science/article/pii/0029554X78907462.

D.P. Barry, G. Leinweber, R.C. Block, T.J. Donovan, Y. Danon, F.J. Saglime, A.M. Daskalakis, M.J. Rapp, and R.M. Bahran, Quasi-Differential Neutron Scattering in Zirconium from 0.5 to 20 MeV, Nuclear Science and Engineering, 174, 2, 188 (2013); 10.13182/NSE12-1., doi:10.13182/NSE12-1..

D. Brown, M. Chadwick, R. Capote, A. Kahler, A. Trkov, M. Herman, A. Sonzogni, Y. Danon, A. Carlson, M. Dunn, D. Smith, G. Hale, G. Arbanas, R. Arcilla, C. Bates, B. Beck, B. Becker, F. Brown, R. Casperson, J. Conlin, D. Cullen, M.-A. Descalle, R. Firestone, T. Gaines, K. Guber, A. Hawari, J. Holmes, T. Johnson, T. Kawano, B. Kiedrowski, A. Koning, S. Kopecky, L. Leal, J. Lestone, C. Lubitz, J. Márquez Damián, C. Mattoon, E. McCutchan, S. Mughabghab, P. Navratil, D. Neudecker, G. Nobre, G. Noguere, M. Paris, M. Pigni, A. Plompen, B. Pritychenko, V. Pronyaev, D. Roubtsov, D. Rochman, P. Romano, P. Schillebeeckx, S. Simakov, M. Sin, I. Sirakov, B. Sleaford, V. Sobes, E. Soukhovitskii, I. Stetcu, P. Talou, I. Thompson, S. van der Marck, L. Welser-Sherrill, D. Wiarda, M. White, J. Wormald, R. Wright, M. Zerkle, G. Žerovnik, and Y. Zhu, ENDF/B-VIII.0: The 8th Major Release of the Nuclear Reaction Data Library with CIELO-project Cross Sections, New Standards and Thermal Scattering Data, Nuclear Data Sheets, 148, 1 (2018); https://doi.org/10.1016/j.nds.2018.02.001., url:http://www.sciencedirect.com/science/article/pii/S0090375218300206, special Issue on Nuclear Reaction Data..

R. Capote, A. Trkov, M. Sin, M. Herman, A. Daskalakis, and Y. Danon, Physics of Neutron Interactions with ^{238}U: New Developments and Challenges, Nuclear Data Sheets, 118, 26–31 (2014); 10.1016/j.nds.2014.04.003..

Chadwick, M., Dupont, E., Bauge, E., Blokhin, R., Bouland, O., Brown, D., Capote, R., Carlson, A., Danon, Y., De Saint Jean, C., Dunn, M., Fischer, U., Forrest, R., Frankle, S., Fukahori, T., Ge, Z., Grimes, S., Hale, G., Herman, M., van der Marck, S., 2014. The CIELO Collaboration: Neutron Reactions on ^{1}H, ^{16}O, ^{56}Fe, ^{235,238}U, and ^{239}Pu. Nucl. Data Sheets 118 (1), 10.

M. Chadwick, R. Capote, A. Trkov, M. Herman, D. Brown, G. Hale, A. Kahler, P. Talou, A. Plompen, P. Schillebeeckx, M. Pigni, L. Leal, Y. Danon, A. Carlson, P. Romain, B. Morillon, E. Bauge, F.-J. Hambsch, S. Kopecky, G. Giorginis, T. Kawano, J. Lestone, D. Neudecker, M. Rising, M. Paris, G. Nobre, R. Arcilla, O. Cabellos, I. Hill, E. Dupont, A. Koning, D. Cano-Ott, E. Mendoza, J. Balibrea, C. Paradela, I. Durán, J. Qian, Z. Ge, T. Liu, L. Hanlin, X. Ruan, W. Haicheng, M. Sin, G. Noguere, D. Bernard, R. Jacqmin, O. Bouland, C. De Saint Jean, V. Pronyaev, A. Ignatyuk, K. Yokoyama, M. Ishikawa, T. Fukahori, N. Iwamoto, O. Iwamoto, S. Kunieda, C. Lubitz, M. Salvatores, G. Palmiotti, I. Kodeli, B. Kiedrowski, D. Roubtsov, I. Thompson, S. Quaglioni, H. Kim, Y. Lee, U. Fischer, S. Simakov, M. Dunn, K. Guber, J. Márquez Damián, F. Cantargi, I. Sirakov, N. Otuka, A. Daskalakis, B. McDermott, and S. van der Marck, CIELO Collaboration Summary Results: International Evaluations of Neutron Reactions on Uranium, Plutonium, Iron, Oxygen and Hydrogen, Nuclear Data Sheets, 148, 189 (2018); https://doi.org/10.1016/j.nds.2018.02.003., url:https://www.sciencedirect.com/science/article/pii/S009037521830022X, special Issue on Nuclear Reaction Data..

Daskalakis, A.M., 2014. Quasi-differential Neutron Scattering from ^{238}U from 0.5 to 20 MeV. Ann. Nucl. Energy 73, 455.

Daskalakis, A.M., 2015. Measurement of Elastic and Inelastic Neutron Scattering in the Energy Range from 0.5 to 20 MeV PhD Thesis. Rensselaer Polytechnic Institute.

Daskalakis, A., Blain, E., McDermott, B., Bahran, R., Danon, Y., Barry, D., Block, R., Rapp, M., Epping, B., Leinweber, G., 2017. Quasi-differential elastic and inelastic neutron scattering from iron in the MeV energy range. Ann. Nucl. Energy 110, 603. https://doi.org/10.1016/j.anucene.2017.07.007. url:http://www.sciencedirect.com/science/article/pii/S0306454917301950.

Daskalakis, A., Blain, E., Leinweber, G., Rapp, M., Barry, D., Block, R., Danon, Y., 2017. Assessment of beryllium and molybdenum nuclear data files with the RPI neutron scattering system in the energy region from 0.5 to 20 MeV. EPJ Web of Conferences 146 (11037), 10.

J.K. Dickens, SCINFUL: A Monte Carlo based computer program to determine a scintillator full energy response to neutron detection for E/sub n/ between 0. 1 and 80 MeV: User's manual and FORTRAN program listing, Technical Report (1988)..

Dunford, C., Holden, N., Pearlstein, S., 2001. CSEWG Symposium, A CSWEG Retrospective. 35th anniversary cross section evaluation working group, NOV. 5, 2001, Brookhaven National Laboratory. (2001); 10.2172/806582..

Haight, R.C., Lee, H.Y., Taddeucci, T.N., O'Donnell, J.M., Perdue, B.A., Fotiades, N., Devlin, M., Ullmann, J.L., Laptev, A., Bredeweg, T., Jandel, M., Nelson, R.O., Wender, S.A., White, M.C., Wu, C.Y., Kwan, E., Chyzh, A., Henderson, R., Gostic, J., 2012. Two detector arrays for fast neutrons at LANSCE. J. Instrum. 7, 03 (C03028), 10.

A. Koning, M. Avrigeanu, V. Avrigeanu, P. Batistoni, E. Bauge, M.-M. Bé, P. Bem, D. Bernard, O. Bersillon, A. Bidaud, O. Bouland, A. Courcelle, C. Dean, P. Dos-Santos-Uzarralde, B. Duchemin, I. Duhamel, M. Duijvestijn, E. Dupont, U. Fischer, and H. Vonach, The JEFF evaluated nuclear data project, doi: 10.1051/ndata:07476 (2008); 10.1051/ndata:07476..

Lisowski, P., Schoenberg, K., 2006. The Los Alamos Neutron Science Center. Nucl. Instrum. Methods Phys. Res., Sect. A 562 (910), 10.

J.E. Lynn, G.H. Kwei, W.J. Trela, V.W. Yuan, B. Cort, R.J. Martinez, and F.A. Vigil, Vibrational properties of Pu and Ga in a Pu-Ga alloy from neutron-resonance Doppler spectroscopy, Phys. Rev. B, 58, 11408 (1998); 10.1103/PhysRevB.58.11408., url:https://link.aps.org/doi/10.1103/PhysRevB.58.11408..

P. Marini, J. Taieb, B. Laurent, G. Belier, A. Chatillon, D. Etasse, P. Morfouace, M. Devlin, J.A. Gomez, R.C. Haight, K.J. Kelly, J.M. O'Donnell, and K.T. Schmitt, Prompt-fission-neutron spectra in the ^{239}Pu(n,f) reaction, Phys. Rev. C, 101, 044614 (2020); 10.1103/PhysRevC.101.044614., url:https://link.aps.org/doi/10.1103/PhysRevC.101.044614..

K.S. Mohindroo, Quasi Differential Neutron Induced Neutron Emission Measurements of ^{235}U and ^{239}, PhD Thesis (2020)url:http://libproxy.rpi.edu/login?url=https://www.proquest.com/dissertations-theses/quasi-differential-neutron-induced-emission/docview/2501480605/se-2?accountid=28525, copyright - Database copyright ProQuest LLC; ProQuest does not claim copyright in the individual underlying works; Last updated - 2021-03-31..

Plompen, A. et al., 2020. The joint evaluated fission and fusion nuclear data library, JEFF-3.3, Eur. Phys. J. A, 56, 7, 181 (2020); 10.1140/epja/s10050-020-00141-9..

Capote, Roberto and Trkov, Andrej, Critical review of CIELO evaluations of n+ 235U, 238U using differential experiments, EPJ Nuclear Sci. Technol., 4, 27 (2018); 10.1051/epjn/2018029., doi:10.1051/epjn/2018029..

F. Saglime, Y. Danon, R. Block, M. Rapp, R. Bahran, G. Leinweber, D. Barry, and N. Drindak, A system for differential neutron scattering experiments in the energy range from 0.5 to 20MeV, Nucl. Instrum. Methods Phys. Res., Sect. A, 620, 2–3, 401 (2010); doi: 10.1016/j.nima.2010.04.051., url:https://doi.org/10.1016/j.nima.2010.04.051..

K. Shibata, O. Iwamoto, T. Nakagawa, N. Iwamoto, A. Ichihara, S. Kunieda, S. CHIBA, K. Furutaka, N. Otuka, T. Ohsawa, T. Murata, H. Matsunobu, A. ZUKERAN, S. Kamada, and J. Ichi Katakura, JENDL-4.0: A New Library for Nuclear Science and Engineering, Journal of Nuclear Science and Technology, 48, 1, 1 (2011); doi:10.1080/18811248.2011.9711675..

Wender, S., Balestrini, S., Brown, A., Haight, R., Laymon, C., Lee, T., Lisowski, P., McCorkle, W., Nelson, R., Parker, W., Hill, N., 1993. A fission ionization detector for neutron flux measurements at a spallation source. Nucl. Instrum. Methods Phys. Res., Sect. A 336, 1, 226. https://doi.org/10.1016/0168-9002(93)91102-S. url:http://www.sciencedirect.com/science/article/pii/016890029391102S.

A.E. Youmans, J. Brown, A. Daskalakis, N. Thompson, A. Welz, Y. Danon, B. McDermott, G. Leinweber, and M. Rapp, Fast Neutron Scattering Measurements with Lead, AccApp 15, Washington, DC, 355–360 (2015)..